Energy Management for Fuel Minimization in Hybrid Fuel Cell All-Electric Aircraft

Modeling, Estimation, and Control of Nonlinear Systems

Diana-Valeria Vacaru

MSc. Thesis - Electronic Systems

September 5, 2025

Aalborg University
Electronics and IT

AALBORG UNIVERSITY
STUDENT REPORT

MSc. Thesis
Electronics and IT
Aalborg University
https://www.aau.dk

Title:
Energy Management for Fuel Minimization in Hybrid Fuel Cell All-Electric Aircraft

Theme:
Modeling, Estimation, and Control of Nonlinear Systems

Project Period:
Spring 2025

Project Group:
Group 1029m

Participant(s):
Diana-Valeria Vacaru

Supervisor(s):
Jakob Stoustrup

Copies: 1

Page Numbers: 45

Date of Completion:
September 5, 2025

Abstract:

This work presents the development and integration of an Energy Management System (EMS) with a propulsion controller for an All-Electric Aircraft powered by a fuel cell, a lithium-ion battery, and a supercapacitor. Offline optimization identifies the optimal fuel cell current and the optimal cruise velocity, which serve as design targets for real-time control. The EMS is implemented as a proportional–integral (PI) controller designed to minimize hydrogen consumption while ensuring that the battery and supercapacitor state of charge (SoC) are depleted exactly at the end of a predefined mission distance. The propulsion PI controller maintains the desired cruise velocity and supplies the propulsion power demand to the EMS. A simplified Matlab model combining the EMS and propulsion dynamics is developed to demonstrate the approach. Simulation results show that the propulsion controller is able to track the aircraft velocity with minimal errors. The EMS on the other hand is not able to efficiently distribute the current between the three components.

Contents

1 | Introduction

As a result of continuous research dedicated to more environmentally friendly solutions for powering All-Electric Aircraft (AEA), fuel cell systems are starting to replace conventional emergency power systems. Fuel cells are capable of highly efficient fuel management, while maintaining lower noise, and significantly less emissions compared to alternatives such as combustion engines. [1] High fuel cell efficiency is possible partly due to their ability to produce electricity directly from chemical energy. The lack of noise is a result of their design which does not consist of moving parts. This property also makes them more reliable, and last longer. Their environmental impact is also deemed considerably low, as undesirable products and emissions are close to zero. [2]

Hybridization of fuel cell systems with batteries and supercapacitors offers significant performance improvements over standalone fuel cell configurations [1]. Since fuel cells exhibit limited efficiency under variable and peak loads, integrating them with batteries and supercapacitors enables operation closer to their optimal conditions. In this hybrid arrangement, the battery supplies supplementary power and stores excess energy, while the supercapacitor addresses high-power demands and handles rapid maneuvers. Assuming ideal efficiency for the battery and supercapacitor (i.e., negligible losses regardless of current levels), the Energy Management System (EMS) can strategically distribute power demands among the three components. A primary objective of this work is to develop such an EMS, and incorporating component constraints to minimize fuel consumption.

To narrow down the scope of the EMS, a specific flight objective is established. The Energy Management System will therefore aid in maximizing the flight distance, later referred to as "fly longer". This objective can be simplified to the following optimization problem: for a given flight distance, minimize fuel consumption.

From a high level perspective, the emphasis is on designing a system-of-systems architecture by integrating multiple components and subsystems. This process involves modeling the aircraft dynamics and aerodynamic constraints, as well as selecting and modeling the EMS components to align with the physical specifications of the aircraft.

First, an offline optimization problem is proposed, see Section 5.1, to determine the optimal aircraft velocity and fuel cell current, which are codependent. Second, a PI controller is proposed to efficiently distribute the current load between the hybrid

system components, as described in Section 3.4. Finally, the aircraft's propulsion system is controlled using classic PI control to track an optimal velocity reference, as detailed in Section 4.3.

The aforementioned leads to the problem statement:

> *How to control an All-Electric Aircraft in order to minimize fuel consumption by optimizing the aircraft's speed and the power distribution of the Energy Management System (EMS) while operating within energy and dynamic constraints?*

Part I

System & Model

2 | System Design

In order to control an AEA such that its fuel consumption is minimized, several subsystems must be designed, modeled, and employed. Fuel consumption is dependent on both the fuel source's efficiency constraints as well as the desired velocity of the aircraft, and the way it is affected by external disturbances such as wind. This combines two systems together, the aircraft and the EMS, both of which must be controlled, resulting in the necessity of designing two controllers. One controller, acting as the main controller, is for propulsion, and the second controller is for the distribution of power between the EMS components. However, on top of the task of load distribution, the EMS must also operate the fuel cell within its current constraints by tracking an optimal fuel cell current. The main goal of the propulsion controller is to track a velocity reference and estimate the amount of power needed to achieve that velocity. These input - output relationships require the addition of another subsystem, one that can estimate the optimal velocity and fuel cell current and also taking their mutual dependency into account. This is achieved by an offline optimization.

To obtain the optimal velocity reference, constraints such as the ones caused by aerodynamic drag have to be taken into consideration. Another constraint is the fuel cell's load current range for optimal performance. In other words the higher the velocity reference, the higher the current load, for which a limit has to be set such that it does not overcome the fuel cell's operational and optimal current limits. To obtain the fuel cell optimal current, specification from the manufacturer's datasheet must be consulted and the relationship between power loss and current has to be found. More details about the offline optimization are presented in Sections 5.1, 3.3.2, and 4.1.

To further explain the proposed solution, a high level representation of the entire system can be found in Figure 2.1. The main controller - the propulsion controller takes as input a velocity reference and outputs the propulsion power needed to reach that reference. In the diagram the output is represented by the current i_{ref} that is in itself a reference to the Energy Management System (EMS) controller. This controller distributes the current load to the energy system components: the fuel cell, battery, and supercapacitor; and outputs a total current applied to the aircraft plant.

The Energy Management System components are described in Section 2.3 and modeled in Chapter 3. The aircraft plant is described in Section 2.2, and modeled in Section 4.2.

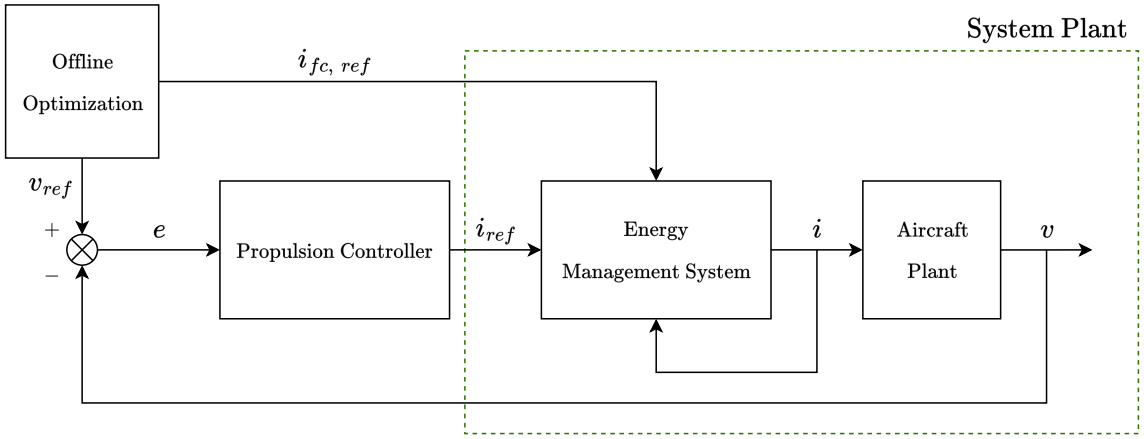

Figure 2.1: System block diagram.

2.1 Mission Objectives

The main focus of the project is to maximize flight endurance by prolonging the flight distance. To simplify this problem, while achieving the same thing, the distance becomes fixed, and the scope is then to use as little fuel as possible for the set distance.

Another major goal is to optimize the Energy Management System to keep the fuel cell operating close to its optimal point ($i_{fc,\,ref}$) by letting the battery and/or the supercapacitor take the remaining current load. The fuel cell is the main source of energy for the aircraft. The battery and the supercapacitor are secondary components used to improve the dynamics and power density of the energy system, allowing for better fuel economy, higher performance, and longer component lifespan. Although, prolonging the lifespan of the components is out of the scope of this work.

The primary roles of the battery are: to store excess energy from the fuel cell during low power flight (e.g. when cruising) and supply it during high power demands (e.g. during takeoff, maneuvering); to maintain constant fuel cell load, within the optimal range, by compensating for fluctuations in power demand; and to act as a backup energy source, which makes the energy system more robust.
The primary roles of the supercapacitor are: to protect the fuel cell and the battery from strain by assisting during sudden power spikes; and to handle events when the battery or the fuel cell cannot respond quickly enough, since they can charge and discharge almost instantly.

In the context of a flight mission, the fuel cell is that component which is used for steady long duration maneuvers where constant amount of current load is necessary. This is true for cruise flight. During takeoff and landing high amounts of power is needed, and this is where the supercapacitor and the battery comes in hand. The fuel cell does not operate well when high bursts of power are necessary, and in order to keep it operating at a steady rate the supercapacitor provides burst power and the battery supplements. During landing the battery can recharge if possible and

the supercapacitor takes on the load alone.

The Energy Management System also has to ensure that the state of charge (SoC) of the battery and supercapacitor is maintained above a certain threshold to avoid full depletion before reaching the final destination.

2.2 Aircraft Configuration

The aircraft model is the same as the one presented in [3], the Avistar UAV aircraft, which can be seen in Figure 2.2, and its geometric properties are presented in Table 2.1.

Figure 2.2: Real representation of the Avistar UAV aircraft [3].

Geometric Properties	
Overall Length	1395 mm (55.0 in)
Wing Span	1590 mm (62.5 in)
Wing Area	43.3 dm^2 (672 in^2)
Aspect Ratio	6.62
Inertial Properties	
Mass/Weight	
Empty (w/o Battery)	3.39 kg (7.46 lb)
4S LiPo Battery	0.53 kg (1.17 lb)
Gross Weight	3.92 kg (8.63 lb)
Wing Loading	90.5 gr/dm^2 (29.6 oz/ft^2)

Table 2.1: Avistar UAV aircraft physical specifications.

2.3 Energy Hybrid System Components

The Energy Management System is composed of a fuel cell, a battery and a supercapacitor.

The model of the battery is taken from [3], which is the battery used to power the exact aircraft presented in Figure 2.2, therefore its size, weight and energy specifications are suitable for the physical specifications of the airplane. The battery model

is called Thunder Power ProLite 3S 1350 mAh, and a commercial option can be found at [4].

The model of the fuel cell is taken from [1] - a liquid cooled Proton-Exchange Membrane (PEM) fuel cell. The numerical data from this paper, as well as from [5], is also used to be able to model the fuel cell, via approximation. However, it is worth mentioning that the exact fuel cell used in this paper is meant to be used for a much larger aircraft. Therefore, the exact data provided cannot be directly used with the small aircraft presented in this work, and would have to be scaled first.

In [1] the fuel cell is also coupled with a battery and a supercapacitor. To scale the supercapacitor and the fuel cell in accordance with the airplane and its battery, the battery proposed in [1] can be linearly scaled to the battery used in [3], see the necessary specifications in Table 2.2. The result of this scaling can be applied to the fuel cell and the supercapacitor.

Battery Specifications		
Parameter	Value	Unit
Large battery		
Nominal Voltage	48	V
Rated Capacity	40	Ah
Battery used		
Nominal Voltage	11.1	V
Rated Capacity	1.350	Ah

Table 2.2: Battery specifications for two models: first taken from [1], second taken from [3].

The scaling factor for current (when voltage is fixed) can be calculated by finding the difference in the batteries' energy in W h:

$$k_s = \frac{11.1\,\mathrm{V} \times 1.350\,\mathrm{A\,h}}{48\,\mathrm{V} \times 40\,\mathrm{A\,h}} = \frac{1}{128} \tag{2.1}$$

The current and voltage can be scaled by the square root of k_s, the reason of which is shown in Equation 2.2.

$$\begin{aligned} E_b &= k_s E_B && [\mathrm{W\,h}] \\ V_{fc}(i_{fc}) i_{fc} &= P_{fc} && [\mathrm{W}] \\ k_s P_{fc} &= k_s (V_{fc}(i_{fc}) i_{fc}) && [\mathrm{W}] \\ k_s E_{fc} &= k_s \int P_{fc} && [\mathrm{W\,h}] \\ \sqrt{k_s} V_{fc}(i_{fc}) \sqrt{k_s} i_{fc} &= k_s P_{fc} && [\mathrm{W}] \end{aligned} \tag{2.2}$$

The fuel cell nominal current and voltage, as well as voltage at 0 A and 1 A can be

approximated by:

$$i_{fc,\,nom} = \sqrt{k_s} I_{nom} \quad [\text{A}] \quad (2.3)$$

$$v_{fc,\,nom} = \sqrt{k_s} V_{nom} \quad [\text{V}] \quad (2.4)$$

$$E_{OC} = \sqrt{k_s} V_0 \quad [\text{V}] \quad (2.5)$$

$$v_{fc,\,1} = \sqrt{k_s} V_1 \quad [\text{V}] \quad (2.6)$$

where $I_{nom}, V_{nom}, E_{OC}, V_1$ are taken from the fuel cell input parameters table presented in [1]. The resulting values for the scaled voltage and current might not reflect reality accurately, however the total power as a result of their multiplication is the measure that matters, and it is the one that fits the physical properties of the aircraft. Additionally, the number of cells N must also be scaled, and to keep things consistent it is also scaled by k_s.

For the initial fuel cell modeling and validation steps, the large model is used, as the papers [1], [5] provide readily available data necessary for testing. Therefore, any graphical representation of the fuel cell, e.g., voltage current relationship, will be using the fuel cell model with 65 cells.

2.4 Initial Available Energy Estimation

To be able to monitor fuel consumption and minimize it, it is necessary to estimate the initial energy for each of the hybrid system components.

The fuel cell chemical energy is given by:

$$E_{chem} = m_{H_2} LHV \quad [\text{J}] \quad (2.7)$$

where:

m_{H_2}	Mass of hydrogen stored	[kg]
LHV	Low heat value of hydrogen of 120×16^6	[J/kg]

The battery initial energy is given by:

$$E_{batt} = 3600 Q V_b \quad [\text{J}] \quad (2.8)$$

where:

Q	Battery capacity	[A h]
V_b	Voltage across the battery	[V]

The supercapacitor initial energy is given by:

$$E_{sc} = \frac{1}{2} C V_{sc}^2 \quad [\text{J}] \quad (2.9)$$

where:

C	Supercapacitor capacitance	[F]
V_{sc}	Voltage across the supercapacitor	[V]

3 | Energy Management System

This chapter contains the models used to develop the simulation of the Energy Management System. The main component of the EMS is the fuel cell, and its model is described in Section 3.3, represented in state-space as well as linearized to be able to simulate it digitally. Due to time constraints the battery and supercapacitor are modeled as integrators, see Sections 3.1-3.2.

3.1 Battery

By modeling the battery as an integrator, the state of charge (SoC) is treated as the integral of battery current over time. This simple model can therefore capture the battery's dynamic behavior of charge and discharge.

The battery charge $it(t)$ is given by Equation 3.1.

$$it(t) = \int_0^t i_b(t)dt \qquad [\text{C}] \quad (3.1)$$

The battery state of charge is given by Equation 3.2. At the end of flight, the SoC should be zero, meaning the battery should be fully depleted.

$$SoC(t) = SoC(t_0) - \frac{it(t)}{Q} \qquad [\%] \quad (3.2)$$

where:

i_b	Battery current	[A]
$it(t)$	Battery charge	[C]
$SoC(t)$	State of charge at time t (between 0 and 1)	
$SoC(t_o)$	Initial charge, at time t_0	
Q	Battery capacity	[A h]

3.2 Supercapacitor

The supecapacitor (SC) can also be modeled by an integrator, where the voltage is treated as the integral of current over time. The dynamic behavior is similar to

the battery, as the supercapacitor's voltage charges or discharges depending on the current.

The voltage across a supercapacitor is given by Equation 3.3, and it should also be equal to zero by the end of flight.

$$V_{sc}(t) = V_{sc}(t_0) - \frac{\int_0^t i_{sc}(t)dt}{C} \quad [\%] \quad (3.3)$$

where:

i_{sc}	Current flowing in or out of the SC	[A]
$V_{sc}(t)$	Voltage across the supercapacitor, at time t	[V]
$V_{sc}(t_o)$	Initial voltage, at time t_0	[V]
C	Capacitance	[F]

3.3 Fuel Cell

The modeling of the fuel cell is based on [5], and [6] (Sections 3.4-3.6). A simplified model for the fuel cell stack is presented in Figure 3.1. For the sake of a better understanding, the model is split into a linear block (inside the dotted rectangle) and a non-linear one.

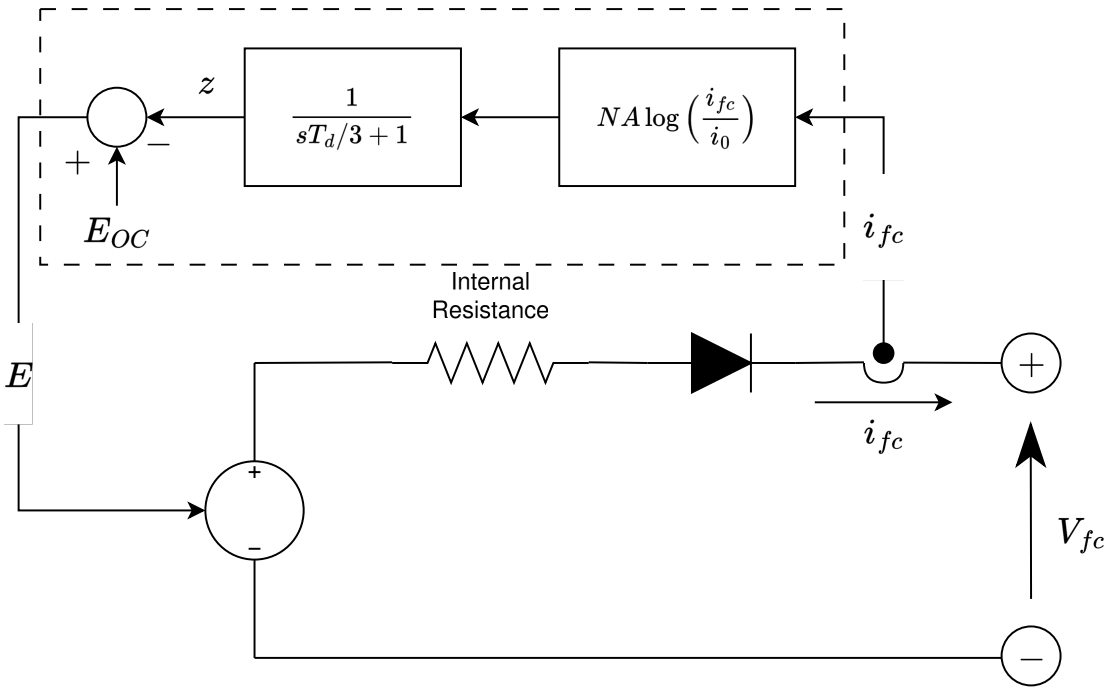

Figure 3.1: Simplified fuel cell stack model.

The controlled voltage source E, which is the output of the linear block, is given by

Equation 3.4. This calculation of voltage considers activation overpotential losses caused by chemical reactions.

$$E = E_{oc} - NAln\left(\frac{i_{fc}}{i_0}\right) \circledast f(t) \quad \text{[V]} \quad (3.4)$$

where $f(t)$ is the time domain representation of $f(s) = \frac{1}{sT_d/3+1}$ which is a transfer function in the frequency domain, added to the model, via convolution ($\circledast$), to represent a voltage delay due to a sudden change in stack current.

The fuel cell stack voltage V_{fc}, which is the output of the non-linear block, is given by Equation 3.5. This models the voltage drop caused by ohmic losses.

$$V_{fc} = E - R_{ohm} i_{fc} \quad \text{[V]} \quad (3.5)$$

where:

E_{OC}	Open circuit voltage	[V]
N	Number of cells	
A	Tafel slope	[V]
i_0	Exchange current	[A]
T_d	Stack settling time at (95% of the final value)	[s]
R_{ohm}	Internal resistance	[Ω]
i_fc	Fuel cell current	[A]
V_{fc}	Fuel cell voltage	[V]

The Tafel equation $Aln\left(\frac{i_{fc}}{i_0}\right)$ holds true only when $i_{fc} > i_0$. For a hydrogen fuel cell the Tafel slope is given by:

$$A = \frac{RT}{n\alpha F} \quad \text{[V]} \quad (3.6)$$

where:

R	Universal gas constant of 8.314472	[J/Kmol]
T	Temperature	[K]
n	Number of moving electrons (n=2)	
α	Charge-transfer coefficient	
F	Faraday's constant of 96485	[A s/mol]

The charge-transfer coefficient α represents the fraction of the applied electrical energy that directly influences the speed of an electrochemical reaction. It's value

depends on the type of reaction and the material used for the electrode, $\alpha \in [0, 1.0]$. For a hydrogen electrode, $\alpha \approx 0.5$, and for an oxygen electrode $\alpha \in [0.1, 0.5]$. It is important to mention that attempting to find an accurate value for A by experimenting with different values for α will have little impact on E, so for this work $\alpha = 0.5$ is used. The term that affects the overpotential the most (described by the Tafel equation) is the exchange current i_0, which increases considerably with temperature. Thus, to keep the activation overpotential as low as possible it is necessary to keep i_0 as low as possible. [6] (Section 3.4.2)

The model in Equations 3.4-3.5 contains a transfer function, which is defined by a frequency domain representation. In order to model the fuel cell digitally it is necessary to bring it to the time (state-space) domain. The steps of converting a transfer function to state-space follows [7] (Section 3.5).

The general transfer function equation is found in Equation 3.7.

$$G(s) = \frac{Z(s)}{R(s)} = \frac{\text{output transform}}{\text{input transform}} \tag{3.7}$$

The linear system relationship between the input and output is described by Equations 3.8-3.9.

$$G(s) = \frac{1}{sT_d/3 + 1} \tag{3.8}$$

$$\Big(\frac{T_d}{3}s + 1\Big)Z(s) = R(s) \tag{3.9}$$

The time domain equivalent of Equation 3.9 is found in Equation 3.10.

$$\frac{T_d}{3}\dot{z} + z = \tilde{u} \tag{3.10}$$

The next step is to isolate $\dot{z}$ from Equation 3.10 as shown in Equation 3.11, where the derivative of the state vector w.r.t time of the linear block is a linear combination of the state and the input to the linear system $\tilde{u}$.

$$\dot{z} = \frac{\tilde{u} - z}{T_d/3} = \frac{3}{T_d}\Big(\tilde{u} - z\Big) \tag{3.11}$$

$$= -\frac{3}{T_d}z + \frac{3}{T_d}\tilde{u} \tag{3.12}$$

The linear system input is given by:

$$\tilde{u} = NAln\left(\frac{i_{fc}}{i_0}\right) \quad \text{[V]} \tag{3.13}$$

The linear system output is given by:

$$\tilde{y} = E = E_{OC} - z \quad \text{[V]} \tag{3.14}$$

As already mentioned the model contains a non-linear part as well, which describes the entire system, therefore it is important to define its input and output. Since the

current of the fuel cell i_{fc} is the one that is being passed as a reference value to the Energy Management System, it is also then considered as an input to the fuel cell model, see Equation 3.15.

$$u = i_{fc} \quad \text{[A]} \tag{3.15}$$

Then the overall fuel cell system state equations are described by Equations 3.16-3.17, where z is replaced by x to emphasize that x represents the entire system, while z represents the system inside the dotted rectangle in Figure 3.1 only. The state variable $x = E_{OC} - E$ represents the stack voltage due to activation losses, which is also delayed.

$$\dot{x} = -\frac{3}{T_d}x + \frac{3}{T_d}NAln\left(\frac{u}{i_0}\right) \tag{3.16}$$

The output V_{fc} is then a function of the input current i_{fc}.

$$y = V_{fc} \tag{3.17}$$
$$= \tilde{y} - R_{ohm}i_{fc} = E - R_{ohm}i_{fc} \tag{3.18}$$
$$= E_{OC} - x - R_{ohm}u \quad \text{[V]} \tag{3.19}$$

According to the model parameter approximation, and validation in [5], the response time T_d, and the open circuit voltage E_{OC} are given, the values of which need to be scaled accordingly. The exchange current is approximated by Equation 3.21, and the internal resistance R_{ohm} by Equation 3.20. The approximations are for steady-state, and for this work these parameters are used during transients as well, in order to simplify things.

$$R_{ohm} = \frac{V_1 - V_{nom} - NAln(I_{nom})}{I_{nom} - 1} \quad [\Omega] \tag{3.20}$$

$$i_0 = \exp\frac{V_1 - E_{OC} + R_{ohm}}{NA} \quad \text{[A]} \tag{3.21}$$

where according to the datasheet of the model in [5]:

V_1	Voltage at 1 A	[V]
V_{nom}	Voltage at nominal operating point	[V]
I_{nom}	Current at nominal operating point	[A]

The Energy Management System requires a control method that can distribute the load between the battery, fuel cell, and supercapacitor. The control method chosen is a Proportional Integral (PI) controller, which is later introduced in Section 3.4. A PI controller is a simple classic method of control, and most design methods for PI control assume linearity. Therefore, the model described by Equations 3.16-3.17 must be linearized.

3.3.1 Linearized Fuel Cell Model

For a non-linear system, the first step in linearization is to decide what the operating point of the model should be and define the incremental variables. Since the input u is part of a non-linear logarithmic function, the linearization should be around u. As defined earlier the state x is chosen to be the voltage caused by activation losses, which is represented by the Tafel equation, therefore also including the logaritmic function. This makes it necessary to linearize around the state x as well.

The next step is to rewrite the linear terms of the mathematical model as a combination of their operating point values and incremental terms defined in equation (3.22).

$$\begin{aligned} x &= \bar{x} + \hat{x} \\ u &= \bar{u} + \hat{u} \end{aligned} \tag{3.22}$$

where:

$\{\bar{x}, \bar{u}\}$ | The operating point

$\{\hat{x}, \hat{u}\}$ | The incremental variables

The result of replacing Equation 3.22 into Equations 3.16-3.17 is:

$$0 = -\frac{3}{T_d}(\bar{x} + \hat{x}) + \frac{3}{T_d} NAln\left(\frac{\bar{u} + \hat{u}}{i_0}\right) \tag{3.23}$$

$$y = E_{OC} - (\bar{x} + \hat{x}) - R_{ohm}(\bar{u} + \hat{u}) \quad [\text{V}] \tag{3.24}$$

Solving for Equation 3.23 gives $x = NAln\left(\frac{u}{i_0}\right)$, which is the voltage due to activation losses.

The non-linear model can be approximated using the Taylor series expansion. For small excursions from x, u to $\bar{x}, \bar{u}$ the higher order terms of the Taylor series can be neglected. This results in a straight line relationship between the change in $\dot{x}(x, u)$ and the excursions away from $\bar{x}, \bar{u}$. The non-linear terms are therefore replaced with first order terms of their Taylor series expansions, using the general formula presented in Equation 3.25 [7] (Section 2.11).

$$f_n(x) - f_n(\bar{x}) \approx \frac{\mathrm{d}f_n(x)}{\mathrm{d}x}\bigg|_{x=\bar{x}} \hat{x} \tag{3.25}$$

Another way of writing it is:

$$\hat{f}(x) \approx m\bigg|_{x=\bar{x}} \hat{x} \tag{3.26}$$

The goal is to bring the state equations into the form:

$$\begin{aligned} \dot{\hat{x}} &= A\hat{x} + B\hat{u} \\ \hat{y} &= C\hat{x} + D\hat{u} \end{aligned} \tag{3.27}$$

where $\hat{x} = x - \bar{x}$ and $\hat{u} = u - \bar{u}$.

Based on Equation 3.25, the state equation can be approximated by:

$$\begin{aligned} \dot{x}(x,u) - \dot{x}(\bar{x},\bar{u}) &= \frac{\partial \dot{x}(\bar{x},\bar{u})}{\partial \bar{x}}\hat{x} + \frac{\partial \dot{x}(\bar{x},\bar{u})}{\partial \bar{u}}\hat{u} = \nabla \dot{x}(\bar{x},\bar{u}) \begin{bmatrix} \hat{x} \\ \hat{u} \end{bmatrix} \\ y(x,u) - y(\bar{x},\bar{u}) &= \frac{\partial y(\bar{x},\bar{u})}{\partial \bar{x}}\hat{x} + \frac{\partial y(\bar{x},\bar{u})}{\partial \bar{u}}\hat{u} = \nabla y(\bar{x},\bar{u}) \begin{bmatrix} \hat{x} \\ \hat{u} \end{bmatrix} \end{aligned} \tag{3.28}$$

Solving for the partial derivatives results in the final linear system:

$$\begin{aligned} \dot{\hat{x}} &= -\frac{3}{T_d}\hat{x} + \frac{3NA}{T_d \bar{u}}\hat{u} \\ \hat{y} &= -\hat{x} - R_{ohm}\hat{u} \end{aligned} \tag{3.29}$$

3.3.2 Fuel Cell Constraints

Hydrogen fuel cells have current ranges (defined by manufacturer specifications) that allow them to work in a more optimal way. Optimal current supply can help prolong the fuel's lifetime and reduce the impact on the fuel cell's life cycle. In this section the focus is on the relationship between the fuel cell power loss and the supplied current.

The fuel cell power loss is also dependent on the fuel cell's efficiency which changes with current. It is important to mention that there are different types of efficiency measures, and in this project the focus is on the electric efficiency. The electric efficiency of a fuel cell stack is defined as the ratio between the stack electric (gross) power and the consumed fuel power as shown in Equation 3.30 [8], [9].

$$\eta_{fc} = \frac{P_{out}}{P_{in}} = \frac{\text{useful electricity produced}}{H_2 \text{ consumed}} = \frac{P_{el}}{P_{H_2,\,consumed}} \qquad [\%] \tag{3.30}$$

To further explain the fuel cell electric efficiency a few components must be explained first. The rate at which the hydrogen is consumed, according to Faraday's law can be described by Equation 3.31 [8]:

$$\dot{n}_{H_2} = \frac{i_{fc}}{nF} \qquad [\text{mol/s}] \tag{3.31}$$

where:

n	Number of electrons transferred per molecule of fuel, where for hydrogen fuel cells, $n = 2$	
F	Faraday's constant of 96485	[C/mol]
$\frac{1}{nF}$	Conversion factor between current i_{fc} in A, and the fuel consumption rate in kg/s	[mol/C]

Given $\dot{n}_{H_2}$, the fuel consumption rate is:

$$\dot{m}_{H_2} = \dot{n}_{H_2} M_{H_2} \quad [\text{kg/s}] \quad (3.32)$$

where M_{H_2} is the molar mass of hydrogen of $0.002\,016\,\text{kg/mol}$.

The energy value of hydrogen consumed $P_{H_2,\,consumed}$ is then:

$$P_{H_2,\,consumed} = \dot{m}_{H_2} LHV = \frac{i_{fc} M_{H_2} LHV}{2F} \quad [\text{W}] \quad (3.33)$$

where LHV is the low heat value of hydrogen equal to 120×10^6 J/kg. This gives the final electric efficiency formula for the stack [9]:

$$\eta_{fc} = \frac{V_{cell}(i_{fc}) 2F}{M_{H_2} LHV} = \frac{V_{cell}(i_{fc})}{1.253\,\text{V}} = \frac{V_{fc}(i_{fc})}{N 1.253\,\text{V}} \quad [\%] \quad (3.34)$$

where N is the number of cells per stack. The electric potential for the stack $V_{fc}(i_{fc})$ is a function of current and can be found using the fuel cell polarization curve as part of the manufacturer's datasheet.

The power loss of the fuel cell can then be estimated using the Equation 3.35, and is dependent on the amount of current supplied.

$$\begin{aligned} P_{fc,\,loss} &= (1 - \eta_{fc}) P_{fc} = P_{in} - P_{out} \\ &= i_{fc} \left(N 1.253\,\text{V} - V_{fc}(i_{fc}) \right) \end{aligned} \quad [\text{W}] \quad (3.35)$$

Then the energy loss of the fuel cell is:

$$E_{fc,\,loss} = P_{fc,\,loss} t = \frac{d}{v} \big(i_{fc} \left(N 1.253\,\text{V} - V_{fc}(i_{fc}) \right) \big) \quad (3.36)$$

where:

d	Flight distance	[m]
v	Flight velocity	[m/s]

3.4 PI Control

In order to distribute the current load between the battery, supercapacitor, and the fuel cell, a simple PI controller is proposed. The consideration of a more advanced control method such as MPC was considered, and determined unnecessary, since MPC works best given future data about the system, and in this case such data is not available. Therefore, it is assumed that a simple PI controller will provide similar results to a MPC controller.

Figure 3.2 provides a representation of the EMS system. The PI controller takes as input the total power demand in form of i_{ref} and the optimal fuel cell current $i_{fc,\,ref}$, and it outputs the current references for the battery and supercapacitor. The output of the plant is the component's actual current delivery $i = i_{sc} + i_b + i_{fc}$. The outputs of each component model are: the supercapacitor voltage V_{sc}, the battery state of charge SoC, and the fuel cell voltage V_{fc}.

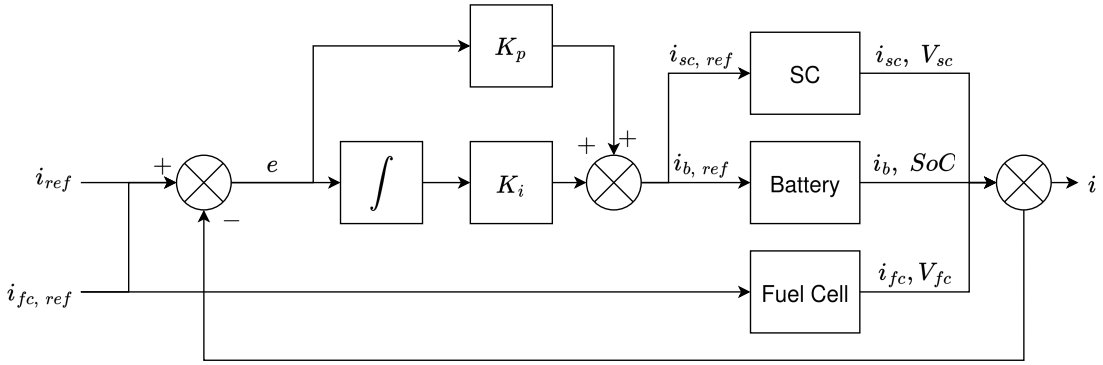

Figure 3.2: Energy Management System block diagram.

The constraints that this controller must keep into account are that the SoC and the V_{sc} must be kept between zero and one, and that they cannot become zero before the end of the simulation. In other words, the battery and supercapacitor cannot be fully depleted before the aircraft reaches the end of the destination.

4 | Propulsion System

This chapter contains the modeling of aerodynamic drag in Section 4.1, as well as of the aircraft plant, see Section 4.2, that describes the relationship between flight velocity and propulsion power, known also as electric power. Additionally, a classic PI control solution is proposed to track an optimal velocity reference, described in Section 4.3.

4.1 Aerodynamic Constraints

Power is required to move an aircraft through the air. When flying, there is an aerodynamic force on the aircraft that is opposite to its velocity vector, also known as air drag. The power generated must overcome this force in addition to achieving a desired velocity. In order to know how much power is needed to overcome the drag, the total drag of a complete airplane must be estimated, and that is not a trivial task. The total drag of an airplane consists of multiple drag forces, the main two being the induced drag and the parasitic drag. The parasitic drag is the total drag minus the induced drag, and in its turn is composed of many other drag components. For the sake of simplicity, this project estimates the skin friction drag, and the form drag only. For a more detailed description of drag, as well as formulas used to estimate the drag forces, consult Chapter 4 in [10].

4.1.1 Skin Friction Drag

The drag caused by viscous shear stresses along the wetted surface of a body is known as skin friction drag. To calculate the skin friction drag it is important to keep in mind the transition between laminar and turbulent flow. This transition is characterized by a gradual shift in fluid behavior from smooth (laminar) to chaotic or irregular (turbulent). Is is influenced by factors like velocity, surface roughness, and it affects the Reynolds number used to calculate the skin friction drag, which will be explained later. During the shift a laminar boundary layer develops at the leading edge of the aircraft part (e.g. wing, fuselage, tail) and at some distance x from that leading edge the laminar boundary becomes unstable and undergoes transition to a turbulent boundary layer. From this x can be defined as the distance from the leading edge to the transition point. [10]

Given the aforementioned, the skin friction drag will be estimated for the laminar flow portion, for the turbulent flow portion, and assuming entirely turbulent flow.

Moreover, the skin friction drag is, among others, dependent on the total wetted area of the aircraft, and for simplicity separate calculations will be made for the main parts of the aircraft such as wings, fuselage and tail, and added together to get the total skin friction drag. The drag estimation requires several geometric properties of the aircraft, and they can be found in Table 2.1, Chapter 2. However, it is important to mention that the table does not include all the necessary precise physical specifications, nor do the sources that provided the table. Therefore, loose approximations were made for the missing data. Table 4.1 contains all the geometric properties necessary to calculate the total drag.

Geometric property	Symbol	Value	Unit
Aspect Ratio	AR	725	-
Oswald efficiency factor	e	0.775	-
Mass	m	3.92	kg
Cruise altitude	h	1520	m
Air density	$\rho(h)$	1.054	kg/m^3
Dynamic viscosity	$\mu(h)$	1.728×10^{-5}	$kg/m \cdot s$
Kinematic viscosity	$\nu(h)$	1.639×10^{-5}	m^2/s
Wing area	A_{wing}	0.433	m^2
Wing span	$Wing_{span}$	20	m
Overall length	$L_{fuselage}$	1.395	m
Mean Aerodynamic Cord (MAC)	$L_{wing} = \frac{A_{wing}}{Wing_{span}}$	0.2723	m
Vertical tail length	$L_{tail} = 0.1 Wing_{span}$	≈ 0.159	m
Fuselage diameter	$D_{fuselage} = \frac{Wing_{span}}{7}$	≈ 0.2271	m
Wing wetted area	$S_{w,\,wing} = 2A_{wing}$	≈ 0.866	m^2
Fuselage wetted area	$S_{w,\,fuselage} = \pi D_{fuselage} L_{fuselage}$	≈ 0.9955	m^2
Tail wetted area	$S_{w,\,tail} = 2 \times 0.1 A_{wing}$	≈ 0.0866	m^2
Fuselage frontal area	$A_{frontal} = \frac{\pi D_{fuselage}^2}{4}$	≈ 0.0405	m^2
Transition distance	x	not constant	m
Wing laminar area	$A_{wing,\,laminar} = x Wing_{span}$	not constant	m^2
Wing laminar wetted area	$S_{w,\,wing,\,laminar} = 2A_{wing,\,laminar}$	not constant	m^2

Table 4.1: Aircraft geometric properties used to calculate air drag.

It is worth to keep in mind that properties such as L_{tail} and $D_{fuselage}$ are visual estimations based on the visual representation of the aircraft seen in Figure 2.2, made in order to be able to carry on with the drag force estimation. It is assumed that in a real scenario such geometric properties will be easily available, and therefore finding accurate values for these is considered irrelevant for the scope of this project, and so the proposed approximations are considered good enough for the intended purposes.

The skin friction drag is a function of the Reynolds number. The Reynolds number based on the total length l is equal to

$$R_l = \frac{vl}{\nu} \tag{4.1}$$

where:

v	Velocity of the aircraft	[m/s]
ν	Kinematic viscosity at an altitude h	[m^2/s]
l	The length of the wing, fuselage or tail	[m]

The kinematic viscosity can be found using Equation 4.2.

$$\nu = \frac{\mu}{\rho} \quad [\text{m}^2/\text{s}] \quad (4.2)$$

The air density at an altitude h can be found using Equation 4.3 [11]:

$$\rho(p, T) = \frac{p}{R_d T} \quad [\text{kg}/\text{m}^3] \quad (4.3)$$

where:

p	Pressure given by Equation 4.4 [11]	[Pa]
T	Air temperature	[K]
R_d	Specific gas constant for dry air of 287.058	[J/kgK]

$$p(h) = p_o \left[\frac{T_0}{T_0 + L_0(h - h_0)} \right]^{\frac{g_0 M}{R L_0}} \quad [\text{Pa}] \quad (4.4)$$

where:

p_0	Standard pressure at sea level of 101325	[Pa]
T_0	Standard temperature at sea level of 288.15	[K]
L_0	Standard temperature lapse rate for subscript 0 of -0.0065	[K/m]
h_0	Altitude at sea level of 0	[m]
R	Molar gas constant of 8.314472	[J/molK]
M	Molar mass of Earth's air of 0.0289644	[kg/mol]
g_0	Gravitational acceleration at sea level of 9.80665	[m/s^2]

The skin friction drag coefficient for turbulent flow can be calculated using Equation 4.5.

$$C_{f,\, turbulent} = 0.455(log_{10} R_l)^{-2.58} \quad (4.5)$$

The skin friction drag is calculated the same for turbulent or laminar flow, see Equation 4.6, and C_f is chosen depending on the flow type. The surface wetted area S_w is chosen based on the aircraft part the drag force is calculated for.

$$D_{Cf} = qC_f S_w \quad [\text{N}] \quad (4.6)$$

The dynamic pressure is given by Equation 4.7.

$$q = \frac{\rho v^2}{2} \quad [\text{N/m}^2] \quad (4.7)$$

The total skin friction drag, if assuming the flow over the aircraft is entirely turbulent, is:

$$D_{Cf,\,turbulent} = D_{Cf,\,turbulent,\,wing} + D_{Cf,\,turbulent,\,fuselage} + D_{Cf,\,turbulent,\,tail} \quad [\text{N}] \quad (4.8)$$

However, the flow over the aircraft is not entirely turbulent, and it is necessary to calculate for the laminar flow as well. For that, the critical distance from the leading edge of the transition point must be calculated, defined by x in Equation 4.9. To calculate for the laminar flow assume a Reynolds transition number of 5×10^5.

$$x = \frac{R_x \nu}{v} \quad [\text{m}] \quad (4.9)$$

The skin friction coefficient for laminar flow can be calculated using Equation 4.10.

$$C_{f,\,laminar} = 1.328 R^{-1/2} \quad (4.10)$$

To calculate the skin friction drag for laminar flow Equation 4.6 is used, where the total wetted area S_w is dependent on the laminar area for the wing and fuselage found as described in Table 4.1.

The total skin friction drag for the laminar part can be found similarly to Equation 4.8.
The next step is to calculate the skin friction drag assuming the flow would be turbulent for the leading portion from the transition point. This can be done by substituting $R_x = 5 \times 10^5$ instead of R_l in equation 4.1. Then in Equation 4.6, the total wetted area S_w is equal to the laminar area for each aircraft part, and the drag is calculated by using the newly calculated skin friction drag coefficient.

Finally the total skin friction drag is calculated by comparing the values for laminar vs turbulent drag over x and calculating the difference between the two. If the resulting difference is larger than the total laminar skin friction drag, then the final skin friction drag equals the drag found by Equation 4.8 minus the difference. Otherwise, the final skin friction drag is equal to the drag found by Equation 4.8 minus the total laminar skin friction drag. To better understand the line of thought in this last paragraph follow the example in [10], Chapter 4, about skin friction drag.

4.1.2 Form Drag

The uneven pressure distribution perpendicular to a body's surface creates form drag. The form drag for the wings and the tail of the aircraft is expected to be much smaller than the skin friction drag due to their shape. Therefore, they are not calculated in this project as their addition might not contribute much to the total drag estimation. Therefore, only the fuselage form drag is calculated. The fuselage of the aircraft does not have a very simple shape and the form drag is usually calculated differently depending on the shape type, and the more complicated the shape the more complicated the form drag estimation. To simplify the calculations, the fuselage was approximated by a cylinder, and in that case the form drag coefficient can be estimated using Equation 4.11.

$$C_d = 3C_f \frac{l}{d} \tag{4.11}$$

where:

d	Diameter of the cylindrical shape	[m]
l	Length of the cylindrical shape	[m]

The form drag can then be calculated using Equation 4.12, where A is the projected frontal area of the fuselage. This area is assumed to be the area of a circle whose radius is set as the maximum diameter of the fuselage.

$$D_{Cd} = qC_dA \quad \text{[N]} \tag{4.12}$$

4.1.3 Parasitic Drag

As mentioned earlier the parasitic drag is calculated by adding the skin friction drag and the form drag.

$$D_{Cd_0} = D_{Cf} + D_{Cd} \quad \text{[N]} \tag{4.13}$$

4.1.4 Lift-induced Drag

Induced drag is caused by the creation of lift on a wing. It occurs because wings generate lift by redirecting airflow downstream, which creates trailing vortices. This drag is not to be avoided, and it is influenced by factors like wing shape, size, and operating conditions.
Since the induced drag is dependent on lift, the expression for lift coefficient is found in Equation 4.14.

$$C_L = \frac{2L}{\rho v^2 S} \tag{4.14}$$

Then the induced drag coefficient is:

$$C_{Di} = KC_L^2 \tag{4.15}$$

where

$$K = \frac{1}{\pi e AR} \tag{4.16}$$

Finally the induced drag is found using the surface wetted area of the wing as in Equation 4.17.

$$D_{Ci} = qC_{Di}S_w \quad \text{[N]} \tag{4.17}$$

4.1.5 Total Drag

The total drag is equal to the parasitic drag plus the induced drag.

$$D = D_{Cd_0} + D_{Ci} \quad \text{[N]} \tag{4.18}$$

Given the total drag the power required to overcome it can be calculated using Equation 4.19:

$$P_{drag} = Dv \quad \text{[W]} \tag{4.19}$$

and subsequently the energy loss due to aerodynamic drag is then:

$$E_{loss,\, air\ drag} = P_{drag}t = P_{drag}\frac{d}{v} = Dv\frac{d}{v} = Dd \quad \text{[J]} \tag{4.20}$$

where d is the flight distance.

4.2 Aerodynamic Modeling

The aerodynamic modeling follows the steps in [3]. Figure 4.1 shows the relationship between the different parts of the aerodynamic system. The model uses as input variables that describe the aircraft's motion such as velocity $\vec{v}$, acceleration $\vec{a}$, turning angle ϕ, and respectively climb angle γ. These variables can be estimated or measured using various sensors. Using the flight mechanics model and given the input variables the thrust power is estimated, which together with the propeller and motor models gives the propulsion power needed for a given velocity reference.

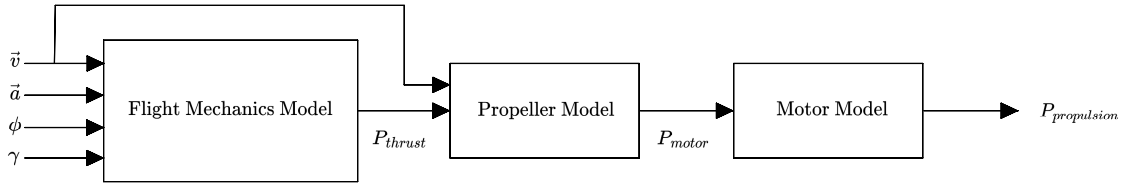

Figure 4.1: Aircraft propulsion power model based on its motion diagram.

4.2.1 Flight Mechanics Model

A simplified overview of the flight mechanics model is presented in this section, and a full version can be found in [3]. The thrust power is equal to the steady state power plus the dynamic power.

$$P_{thrust} = P_{ss} + P_{dyn} \quad \text{[W]} \quad (4.21)$$

The dynamic power follows the Newton's second law as follows:

$$P_{dyn}(\vec{a}, \vec{v}) = m(\vec{a} \cdot \vec{v}) \quad \text{[W]} \quad (4.22)$$

The steady state power considering non constant lift-to-drag ratio, affected by the lift $L = W\frac{cos\gamma}{cos\phi}$, where $W = mg$, is found in Equation 4.23.

$$P_{ss} = K_p v^3 + K_i \frac{cos^2\gamma}{v cos^2\phi} + mgvsin\gamma \quad \text{[W]} \quad (4.23)$$

The K_p and K_i constants are defined by:

$$K_p = \frac{1}{2}\rho S C_{D_o} \quad \text{[kg/m]} \quad (4.24)$$

and

$$K_i = \frac{2Km^2g^2}{\rho S} \quad \text{[kgm}^3\text{/s}^4\text{]} \quad (4.25)$$

with the geometric properties S, m presented in Table 4.1. The constant aerodynamic coefficient K was previously introduced in Equation 4.16, and the parasitic drag coefficient defined in Equation 4.13.

Equation 4.26 relates the propulsion power to the thrust power, accounting for propeller and motor efficiencies.

$$P_{propulsion} = \frac{P_{thrust}}{\eta_p \eta_m} \quad \text{[W]} \quad (4.26)$$

4.2.2 Propeller Model

The commercial model used is the Aero-Naut CAM carbon folding 13x6.5 propeller, which is is a 13-inch diameter propeller with a pitch of 6.5 inch/revolution. More details about it can be found in the UIUC Propeller Database - Volume 3 [12].

To model the propeller, it is necessary to model its efficiency. The propeller efficiency varies highly when using the same propeller, and it is equal to:

$$\eta_p = \frac{C_T}{C_P} J \quad [\%] \quad (4.27)$$

where:

C_T	Thrust coefficient
C_P	Power coefficient
J	Advance ratio

The propeller efficiency, the thrust and power coefficients are all function of J. This relationship can be found from the propeller database of the specific model, see Figure 4.2.

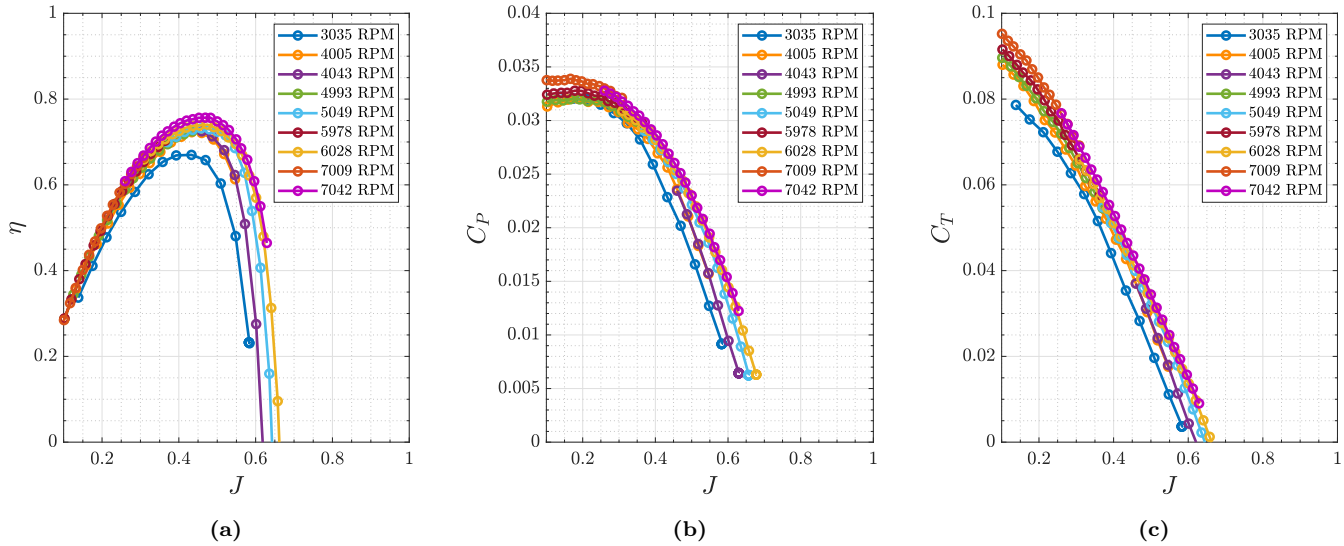

Figure 4.2: Performance characteristics of the Aeronaut CAM 13 × 6.5 propeller [12]: (a) Efficiency η, (b) Power coefficient C_P, and (c) Thrust coefficient C_T as functions of advance ratio J for various RPM settings.

The advance ratio J is equal to:

$$J = \frac{v}{nD} \tag{4.28}$$

where:

v	Velocity of the aircraft	[m/s]
n	Angular velocity	[rad/s]
D	Diameter of the propeller	[m]

As J is dependent on the angular velocity n which changes w.r.t. current applied on the motor attached to the propeller, a way to calculate n can be found in Equation 4.29. As n in this equation depends on the propulsion power, which is dependent on the propeller efficiency η_p an iterative approach must be used to calculate for n.

$$n = \sqrt[3]{\frac{P_{propulstion}}{C_P \rho D^5}} \quad \text{[rad/s]} \tag{4.29}$$

Once J is available, corresponding values for η_p can be found through interpolation, using the relationships provided by the manufacturer as seen in Figure 4.2a.

4.2.3 Motor Model

The motor connected to the propeller is called Model Motors AXi Cyclone 46/760, which is a brushless DC-motor [3], [13]. The impact of the motor on the propulsion power can be defined in terms of motor efficiency which can be estimated using Equation 4.30. Table 4.2 contains several specifications that are needed for the following calculations.

Geometric property	Symbol	Value	Unit
Motor current at zero load	i_0	1.3	A
Motor speed constant	K_v	760	rpm/V
Motor internal resistance	R	0.062	Ω

Table 4.2: Model Motors AXi Cyclone 46/760 specifications [14].

The motor efficiency, which is known to remain relatively constant when using the same propeller, is then:

$$\eta_m(\Omega, U_m) = \Big(1 - \frac{i_0 R}{U_m - \Omega/K_v}\Big)\frac{\Omega}{U_m K_v} \quad [\%] \quad (4.30)$$

where:

U_m	Terminal voltage	[V]
Ω	Angular velocity	[rad/s]

The terminal voltage is controlled using pulse width modulation (PWM), by scaling down the electric potential on the bus by using the throttle percentage t_{pwm} known in other applications as the duty cycle.

$$U_m = t_{pwm} U_{bus}, \quad t_{pwm} \in [0, 1] \quad [\text{V}] \quad (4.31)$$

For this project the assumption is that the DC-to-DC converters are taking care of the voltage conversion between the hybrid system components and the bus, which makes it possible for the components to have their own internal voltages that differ from each other. This is out of the scope of this project, therefore, to simplify things, the bus voltage is considered constant and chosen to be close to the nominal voltage of the hybrid system.

The throttle percentage is not constant, when the velocity reference is not constant, as it is indirectly connected to the aircraft's acceleration. Depending on the throttle percentage input there can be more voltage, therefore more current and thus more power released, which affects the aircraft's acceleration. In this project the assumption is that the power electronics is working and so the relationship between $\vec{a}$ and t_{pwm} is not modeled. Its direct input to the dynamic model of the plant is also omitted, because it is implicitly inputted by the current load being passed into the controller in form of propulsion power as in $i_{load}\, U_m$.

4.2.4 Final Propulsion Power Model

The propulsion power model for non-constant lift-to-drag ratio is:

$$P_{propulsion} = K_p \frac{v^3}{\eta_p \eta_m} + K_i \frac{\cos^2 \gamma}{\eta_p \eta_m v \cos^2 \phi} + mg \frac{v \sin \gamma}{\eta_p \eta_m} + m \frac{\vec{a} \cdot \vec{v}}{\eta_p \eta_m} \quad [\text{W}] \quad (4.32)$$

Using Equation 4.32 the acceleration of the aircraft can be estimated, assuming the acceleration and velocity vectors $\vec{a}, \vec{v}$ are collinear, which they are during cruise flight, which represents the most part of the flight path.

$$a = \frac{1}{mv}(P_{propulsion} \eta_p \eta_m - K_p v^3 + K_i \frac{\cos^2 \gamma}{v \cos^2 \phi} - mgv \sin \gamma) \quad [\text{m/s}^2] \quad (4.33)$$

The velocity of the aircraft can be estimated from acceleration as seen in Equation 4.34.

$$v = \int_0^t \frac{1}{mv}(i_{load} U_{bus} \eta_p \eta_m - K_p v^3 + K_i \frac{\cos^2 \gamma}{v \cos^2 \phi} - mgv \sin \gamma) \quad [\text{m/s}] \quad (4.34)$$

4.2.5 Linearized Propulsion Power Model

The dynamic equation is presented in Equation 4.35, where the state is defined by $x = v$, the input is defined by $u = i_{load}$, and the output is the same as the state, $y = v$.

The relationship between current and voltage is nonlinear, and so is the velocity component, therefore the operating point is chosen to be $\{\bar{v}, \bar{i}\}$, and the incremental variables $\{\hat{v}, \hat{i}\}$.

$$\dot{v} = \frac{1}{mv}(i_{load} U_{bus} \eta_p \eta_m - K_p v^3 + K_i \frac{\cos^2 \gamma}{v \cos^2 \phi} - mgv \sin \gamma) \quad [\text{m/s}^2] \quad (4.35)$$

Here the terms η_p and K_p are functions of velocity v, therefore it is important to expand Equation 4.35 such that it includes all velocity terms.

The propeller efficiency is given by:

$$\eta_p(v) = \frac{vC_T}{nDC_P} \quad (4.36)$$

The K_p constant is given below and will be further expanded given C_{D0} in Equation 4.39.

$$\begin{aligned} K_p(v) &= \frac{1}{2}\rho S C_{D0}(v) = \frac{1}{2}\rho S(C_f(v) + C_d(v)) \\ &= \frac{1}{2}\rho S\Big(C_f(v) + 3C_f(v)\frac{l}{d}\Big) \qquad [\text{kg/m}] \end{aligned} \quad (4.37)$$

The skin friction coefficient is a function of velocity due to the Reynolds number's dependency on v, given by Equation 4.1. The Reynolds number used to calculate $C_{f,\,laminar}$ is chosen to be 5×10^5.

$$C_f(v) = C_{f,\,turbulent} - C_{f,\,laminar} = 0.455\Big(log_{10}\frac{vl}{\nu}\Big)^{-2.58} - 1.328R^{-1/2} \quad (4.38)$$

The parasitic drag coefficient as a function of velocity is given by:

$$\begin{aligned} C_{D0}(v) = \frac{3l}{d}0.455\Big(log_{10}\frac{vl}{d}\Big)^{-2.58} - \frac{3l}{d}1.328R^{-1/2} + \\ + 0.455\Big(log_{10}\frac{vl}{d}\Big)^{-2.58} - 1.328R^{-1/2} \end{aligned} \tag{4.39}$$

Given Equations 4.36-4.39, the aircraft's acceleration can then the described by Equation 4.40.

$$\begin{aligned} \dot{v} =& \frac{i_{load}U_{bus}C^T\eta_m}{mC_PnD} - \frac{3v^2l\rho S}{2md}0.455\Big(log_{10}\frac{vl}{\nu}\Big)^{-2.58} + \\ &+ \frac{3v^2l\rho S}{2md}1.328R^{-1/2} - \frac{v^2\rho S}{2m}0.455\Big(log_{10}\frac{vl}{\nu}\Big)^{-2.58} + \\ &+ \frac{v^2\rho S}{2m}1.328R^{-1/2} + \frac{K_i}{mv^2}\frac{cos^2\gamma}{cos^2\phi} - gsin\gamma \qquad [\mathrm{m/s^2}] \end{aligned} \tag{4.40}$$

The next step is to linearize Equation 4.40, using the Taylor series expansion method presented in Equation 3.25.

$$\dot{v}(v,i) = \dot{v}(\bar{v},\bar{i}) + \frac{\partial\dot{v}(\bar{v},\bar{i})}{\partial\bar{v}}\hat{v} + \frac{\partial\dot{v}(\bar{v},\bar{i})}{\partial\bar{i}}\hat{i} = \dot{v}(\bar{v},\bar{i}) + \nabla\dot{v}(\bar{v},\bar{i})\begin{bmatrix}\hat{v}\\ \hat{i}\end{bmatrix} \tag{4.41}$$

The final linearized propulsion power model is given by Equation 4.2.5.

$$\begin{aligned} \hat{\dot{v}}(\hat{v},\hat{i}) =& \Big(- \frac{1.365l\rho S\bar{v}}{md}(log_{10}\frac{\bar{v}l}{\nu})^{-2.58} + \frac{3.5217\ l\rho S\bar{v}}{2md\ ln(10)}(log_{10}\frac{\bar{v}l}{\nu})^{-3.58} - \\ &- \frac{0.455\rho S\bar{v}}{m}(log_{10}\frac{\bar{v}l}{\nu})^{-2.58} + \frac{1.1739\ \rho S\bar{v}}{2m\ ln(10)}(log_{10}\frac{\bar{v}l}{\nu})^{-3.58} + \\ &+ \frac{3.984\ l\rho S\bar{v}}{md}R^{-1/2} + \frac{1.328\ \rho S\bar{v}}{m}R^{-1/2} - \\ &- \frac{2K_i}{m\bar{v}^3}\frac{cos^2\gamma}{cos^2\phi}\Big)\hat{v} + \Big(\frac{U_{bus}C_T\eta_m}{mC_PnD}\Big)\hat{i} \qquad [\mathrm{m/s^2}] \\ \hat{y} =& \hat{v} \qquad [\mathrm{m/s}] \end{aligned} \tag{4.42}$$

4.3 PI Control

To ensure the aircraft accurately follows a velocity reference, a feedback controller is necessary. A complicated system such as the one presented in Equations 4.40 and 4.42 requires a more advanced control technique such as Model Predictive Control (MPC), that is able to use future data, such as wind predictions, in order to track a reference and tackle disturbances. Nevertheless, due to time constraints this work employs a classical PI controller instead.

The model used for this controller is the linearized aircraft plant previously introduced in Equation 4.42. This sets the necessity for choosing an operating point.

The operating point represents the system in steady-state, i.e. $\dot{v} = 0$, and the one chosen for the implementation of the controller is $\{\bar{v}, \bar{i}\} = \{12, \bar{i}(\bar{v})\}$. The velocity of 12 m/s is the reference optimal velocity for cruise flight. During cruise flight, assuming ideal conditions such as no wind or other disturbances, the velocity is constant, meaning that the acceleration is zero. Therefore, the optimal velocity value is considered a suitable operating point value. The operating point for current is chosen as a function of velocity, and computed numerically using Equation 5.6.

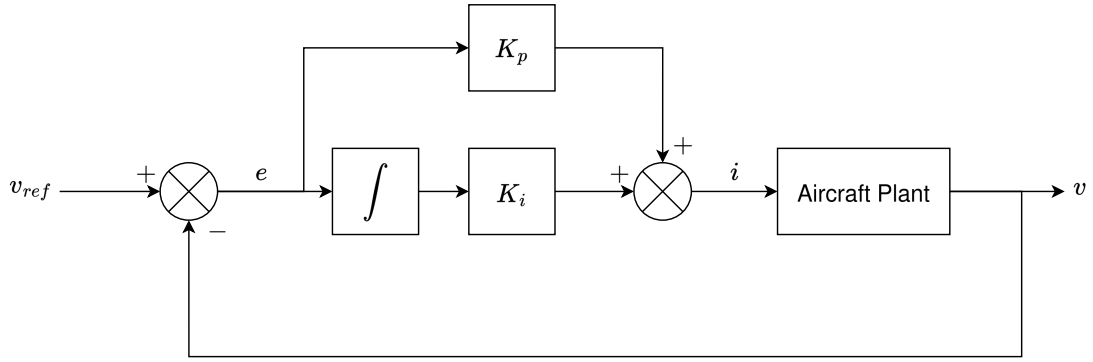

Figure 4.3: PI propulsion controller block diagram.

The system described in Equation 4.42 is a first order system. This would make an extra derivative term for the controller irrelevant since the derivative action is mainly useful for high order dynamics. Therefore a proportional integral controller is deemed enough for this type of system. The proportional term shapes how fast and how strongly the system reacts, and the integral term eliminates steady-state error.

Given the operating point chosen, the A and B coefficients of the state space linear system can be estimated. If A is negative, that means the system is naturally stable, requiring a small proportional gain K_p. If A is positive, that means the system is unstable, requiring for a large K_p to overcome the instability. The integral gain K_i does not depend directly on A. The B coefficient determines the impact the input has on the plant. If B is small, meaning the actuator is weak, the controller requires larger K_p, K_i gains, and vice versa for a large B. In the case of this propulsion system, A is negative, and B is small and positive. Therefore, this requires large integral and proportional gains. The controller simulation and results are presented in Chapter 6.

5 | System-wide Optimization

5.1 Optimal Velocity and FC Current

As previously mentioned, when flying the aircraft encounters a force called aerodynamic drag, which requires power to counteract, and the more drag the more power is required. The relationship between power loss due to aerodynamic drag is explained in Section 4.1. To achieve this power a certain current must be supplied from the hybrid energy system. The battery and supercapacitor do not have current constraints that affect the energy losses, unlike the fuel cell. This means that there is a need to estimate the optimal fuel cell current such that the power loss from the fuel cell is minimized. According to Figure 5.1b, the power loss (estimated using Equation 3.35 and the relationship between voltage and current seen in Figure 5.1a) grows linearly with current, with a minimum loss at zero current. As zero current load is not possible, this means the current should be kept as low as possible.

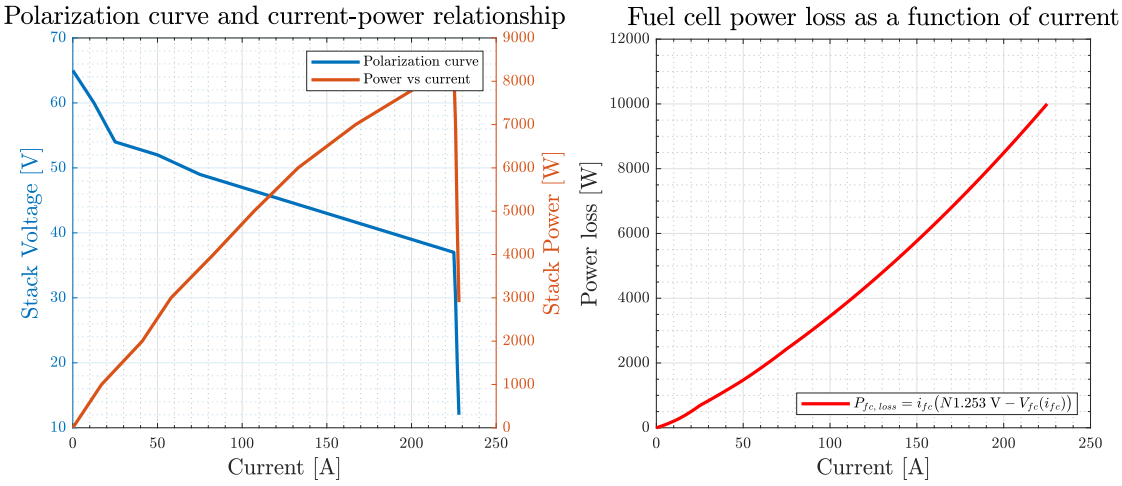

(a) Voltage decreases with current, while power rises to a peak before falling at higher currents.

(b) Power losses grow approximately linearly with current.

Figure 5.1: Comparison of fuel cell operating characteristics. The left plot shows how voltage $V_{fc}(i_{fc})$ decreases and power output peaks as current i_{fc} increases, while the right plot highlights the growth of power losses at higher current levels.

The optimal fuel cell current can be found using Equation 5.1. Here the current is the independent variable, and the voltage is a function of current, which can be found using the polarization curve (the blue curve) in Figure 5.1a, which can be found from the fuel cell's manufacturer datasheet.

$$i_{fc,\,ref} = \arg\min_{i_{fc}}(E_{fc,\,loss}) = \arg\min_{i_{fc}}\left(\frac{d}{v}\left(i_{fc}\left(N1.253\,\mathrm{V} - V_{fc}(i_{fc})\right)\right)\right) \quad [\mathrm{A}] \quad (5.1)$$

where:

d	Flight distance	[m]
v	Flight velocity	[m/s]
N	Number of cells per stack	

The power is not the only entity dependent on current, but so is the aircraft's velocity. In this case the dependency is reciprocal. And as shown in Figure 5.2 the power is also dependent on velocity.

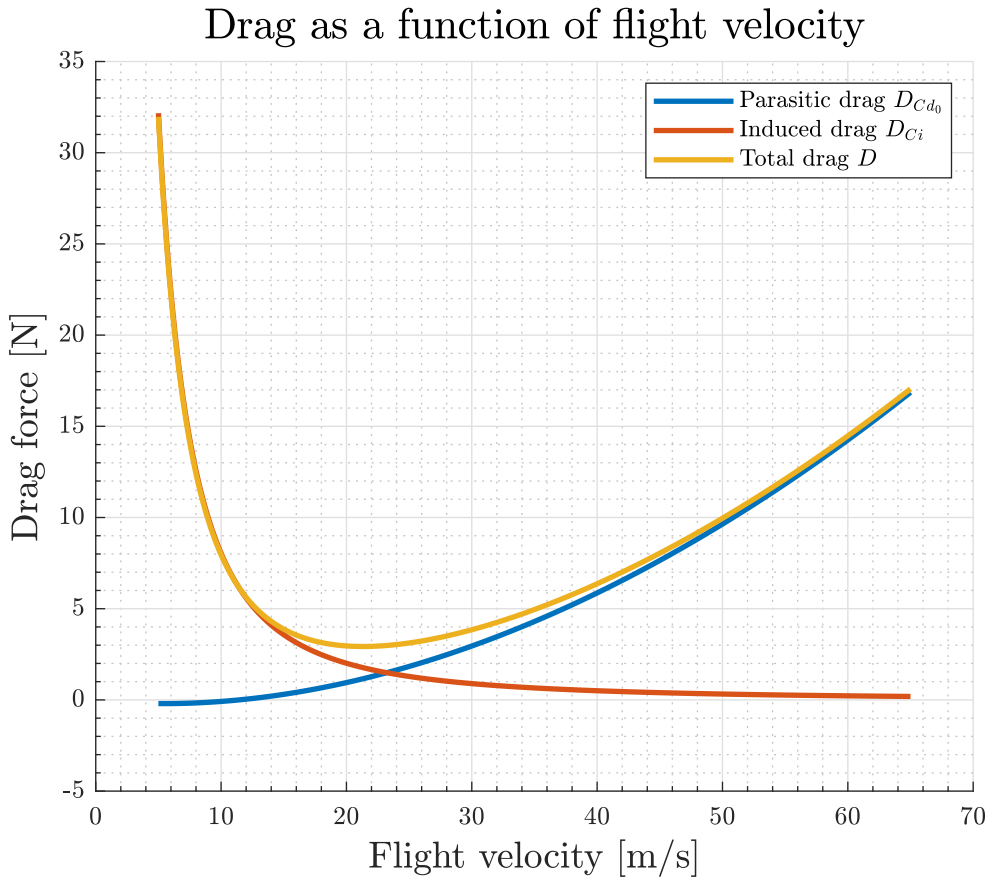

Figure 5.2: Parasitic drag increases with velocity, induced drag decreases, and their sum yields the total drag curve.

Given the aforementioned, the estimation of the optimal velocity V_{opt} and of the optimal fuel cell current $i_{fc,\,ref}$ must be done via a joint optimization problem, as both V_{opt} and $i_{fc,\,ref}$ depend on one another. The objective function is defined in Equations 5.2-5.3.

$$[V_{opt}, i_{fc,\,ref}] = \arg\min_{i_{fc},\,v}(E_{air\ drag,\,loss} + E_{fc,\,loss}) \tag{5.2}$$

$$= \arg\min_{i_{fc},\,v}\left(\frac{d}{v}\Big(i_{fc}\big(N1.253\,\mathrm{V} - V_{fc}(i_{fc})\big) + P_{drag}\Big)\right) \quad [\mathrm{m/s},\ \mathrm{A}] \tag{5.3}$$

The relationship between the current i_{fc} and the velocity v is given by the propulsion power equation for steady-state case ($a = 0, \gamma = 0, \phi = 0$):

$$P_{propulsion} = i_{fc}V_{fc}(i_{fc}) = K_p\frac{v^3}{\eta_p\eta_m} + K_i\frac{1}{\eta_p\eta_m v} \quad [\mathrm{W}] \tag{5.4}$$

The voltage $V_{fc}(i_{fc})$, for steady-state case, can be written in terms of i_{fc} based on Equations 3.4-3.5 rewritten for the convenience of the reader in Equation 5.5:

$$V_{fc}(i_{fc}) = -R_{ohm}i_{fc} + E_{OC} - NAln\Big(\frac{i_{fc}}{i_0}\Big) \quad [\mathrm{V}] \tag{5.5}$$

Given Equations 5.4-5.5, the current i_{fc}, or the velocity v, can be isolated using the following relationship:

$$K_p\frac{v^3}{\eta_p\eta_m} + K_i\frac{1}{\eta_p\eta_m v} = -R_{ohm}i_{fc}^2 + E_{OC}i_{fc} - NAln\Big(\frac{i_{fc}}{i_0}\Big)i_{fc} \tag{5.6}$$

The equation above is solved numerically for v, and for i_{fc}. The results are checked by calculating the value of $V_{fc}(i_{fc})$ from the right hand side of the equation using another method. That is by interpolating, for the input i_{fc}, the polarization curve from the datasheet of the fuel cell.

Due to time constraints the offline optimization is solved numerically, by checking the global minimum of the total energy loss against velocity, and against current. The result is presented in Section 6.1.

Part II

Simulation & Results

6 | Nonlinear Simulation

This chapter includes simulations of the dynamic models, with comments about the results relative to what was expected. Further comments are also presented in Section 7.1.

6.1 Estimating optimal velocity and FC current

This section contains the results of the nonlinear offline optimization presented in Section 5.1. In addition to that, a description of the sanity of the results is also provided.

As already mentioned the offline optimization is solved numerically, using the plots in Figure 6.1. The optimal velocity and fuel cell current are found from the graphs as the minimum points on the blue curves, representing the total energy loss w.r.t. current and velocity. In Equation 5.3, the minimum is calculated as the minimum of the energy loss due to air drag together with the energy loss due to the fuel cell's behavior at certain currents. Therefore, plotting the total relationship should also graphically show which one is the minimum. To check for its correctness, the individual plots for air drag and fuel cell energy loss are also plotted, and in both plots it can be observed that the optimal points (the red dots) are in between the red and green curves, as expected.

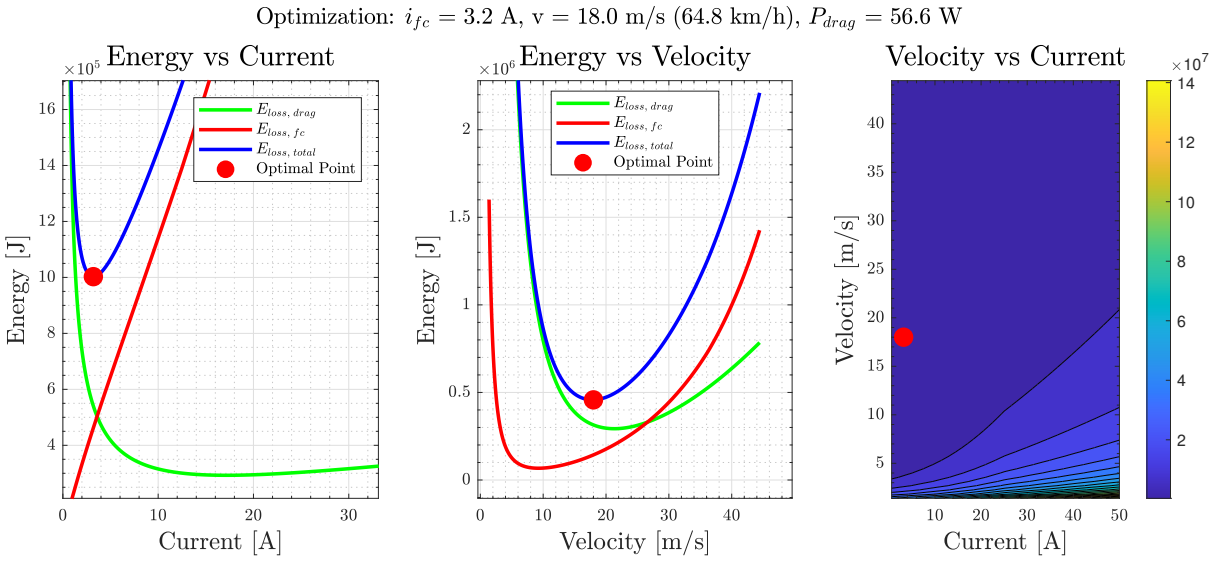

Figure 6.1: Offline optimization: optimal velocity and fuel cell current.

In the left most plot, the green curve represents the energy loss due to air drag as a function of current. For lower currents (but not the lowest) the energy loss due to air drag is lowest, after which it starts to increase with higher current, gradually at first, and then more rapidly. This graph also shows that for very low currents, there is a considerably large energy loss, which does not make sense, since at low currents the aircraft would fly very slowly, which would cause low air drag and consequently low energy loss due to air drag. This means that the modeling is not able to properly represent the real physical system at very low currents. This is probably caused by some approximations in the model, such as the parasitic drag coefficient, which is a function of velocity, and for the sake of simplicity was left constant. Nevertheless, this inconsistency in modeling is deemed to not have a strong impact on the result of the optimization, and therefore is left as it is.

The red curve represents the energy loss related to the fuel cell. The relationship between energy loss and current seems to be linear, based on this plot, and it is caused by substantially large energy loss values. For a closer visual representation see Figure 6.2. The energy loss increases with current, showing that the fuel cell operates best at very low currents.

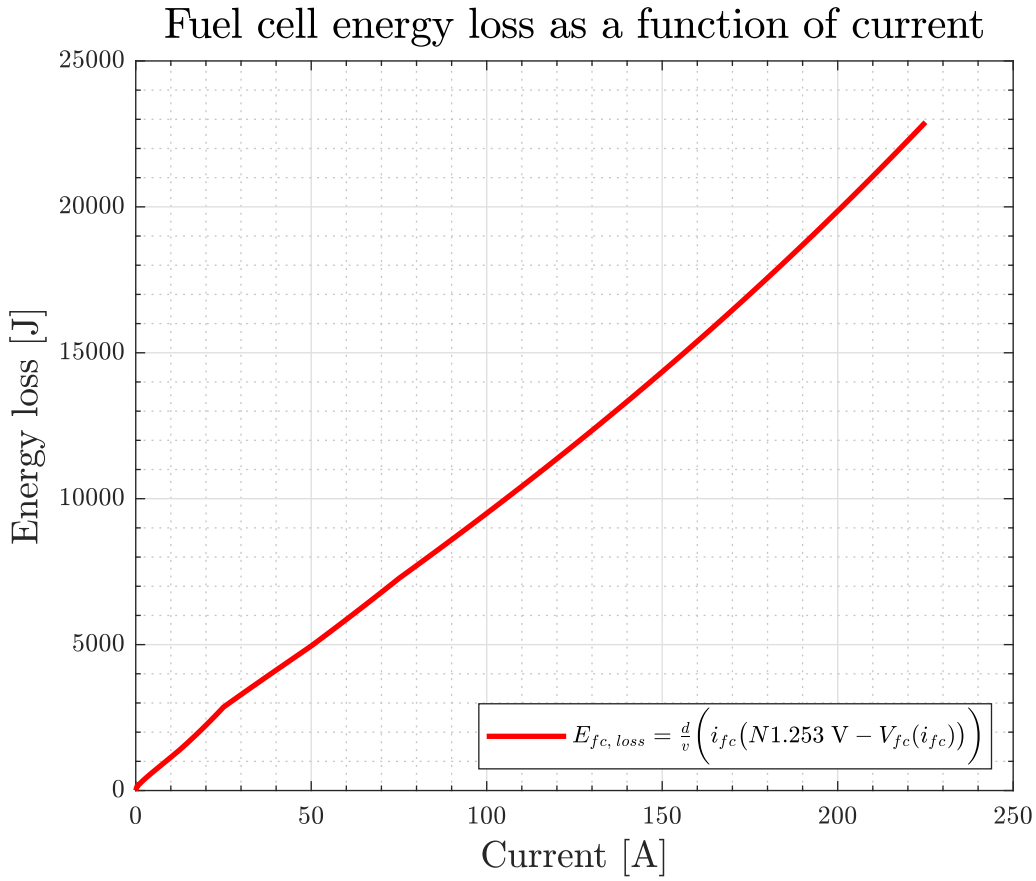

Figure 6.2: Fuel cell energy loss grows nonlinearly with current.

In the middle plot in Figure 6.1, the energy loss is a function of velocity. The energy loss due to air drag increases with velocity as expected. The energy loss related to the fuel cell also increases with velocity, because higher velocity requires higher current, and as established, the fuel cell has major energy losses at high currents.

It is necessary to mention that the numerical method treats i_{fc} and v independently, which does not provide a global solution for the objective function presented in Equation 5.3. A solution for that could be to pick only one of these parameters, either i_fc or v, and calculate the other one using their relationship formula mentioned in Equation 5.6. Thus, for a current $i_{fc} = 3.2\,\mathrm{A}$ the corresponding velocity is $v = 12.27\,\mathrm{m/s} = 44.16\,\mathrm{km/h}$.

The relationship between current and velocity is analyzed by looking at Figures 6.3a and 6.3b. The velocity grows nonlinearly with current as expected. In other words the more current is supplied, the faster the aircraft can fly. In Figure 6.3b, the current grows exponentially with velocity, due to the cubic term v^3, and it saturates at some point. This saturation is believed to be caused by the current reaching its maximum, given the fuel cell parameters such as the number of cells, open circuit voltage, internal resistance, and exchange current.

Given the aforementioned, the modeling of the relationship between voltage and

current is deemed a close approximation to its real physical behavior.

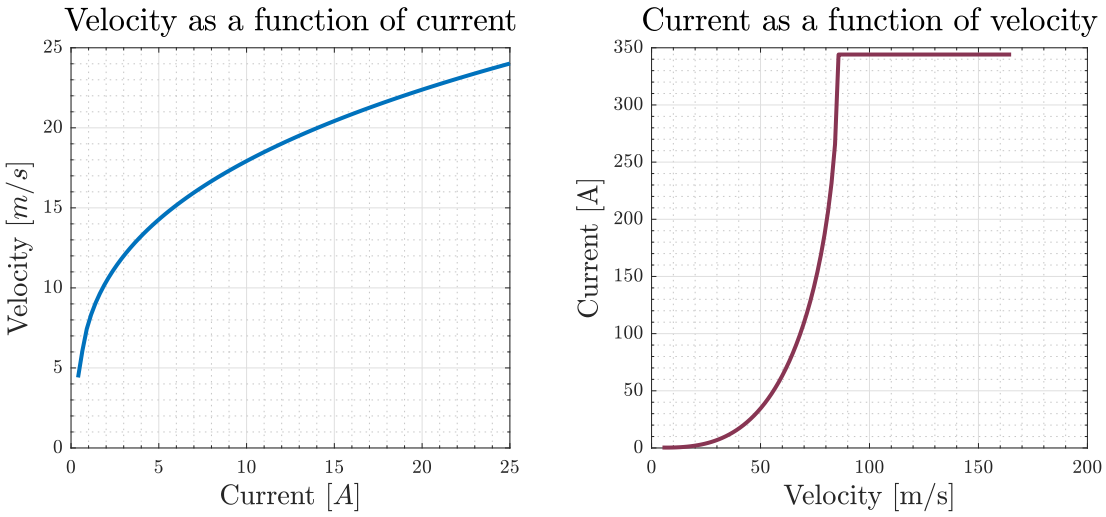

(a) Velocity increases nonlinearly with current.

(b) Current increases exponentially with velocity until it reaches a maximum.

Figure 6.3: Nonlinear relationship between velocity and current in an electric propulsion system: (a) Velocity vs. Current, (b) Current vs. Velocity.

Finally, the result for optimal velocity of $v = 12.27\,\mathrm{m/s}$ as a function of current is determined to be a more suitable velocity for a small airplane of only $3.92\,\mathrm{kg}$, as provided in Table 2.1. Therefore, the final result of the offline optimization is $i_{fc,\,opt} = 3.2\,\mathrm{A}$ and $v_{opt} = 12.27\,\mathrm{m/s}$.

6.2 Integrated System Simulation

This section is dedicated to the integration and simulation of all three subsystems.

The EMS component scaling method proposed in Section 2.3 does not seem to provide realistic approximations. Therefore, the data for the large fuel cell presented in [1] is used during the simulations. This is why the controller output in Figure 6.4b reaches high values all the way up to $\approx 170\,\mathrm{A}$. The computed propulsion current ramps up during acceleration to reach the optimal velocity of $12\,\mathrm{m/s}$, and decreases during deceleration. This shows that the current is delivering an appropriate current profile for the velocity reference.
The velocity converges quickly to the reference value and continues to stay so with minimal errors. However, as noticed in Figure 6.4, there are two spikes in the tracking velocity error plot which correspond to the transients. This error is most likely caused by the approximation made in 4.33, where $\bar{a}, \bar{v}$ are assumed collinear. This relationship is however not collinear at transients, therefore the current model is not able to accurately model for these changes in acceleration.

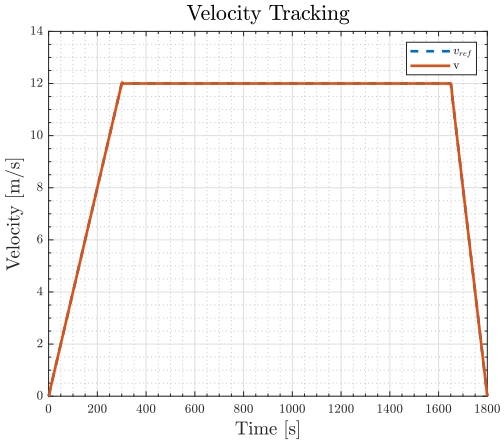

(a) Actual velocity response.

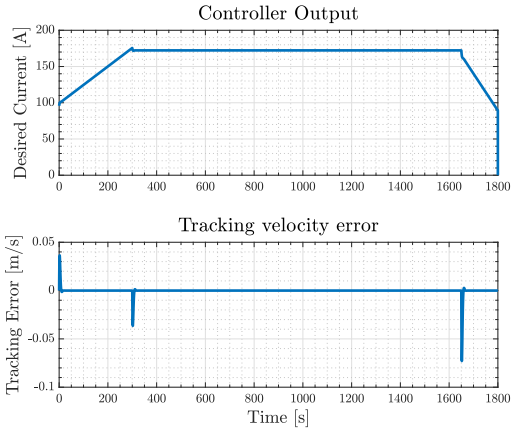

(b) Up: Output propulsion current, during acceleration, steady cruise, and deceleration phases. Down: Velocity tracking error, showing small deviations only during acceleration and deceleration transients.

Figure 6.4: Propulsion controller state, output and tracking error.

The output of the propulsion system i_{ref} is passed on to the EMS system, in form of an input reference. The second input reference is $i_{fc,\,ref}$ which is the result of the offline optimization. According to Figure 6.5a the fuel cell is able to follow its optimal reference. However, the battery discharges prematurely and does not get recharged by the fuel cell. Thus, it is not able to follow the remaining current reference.

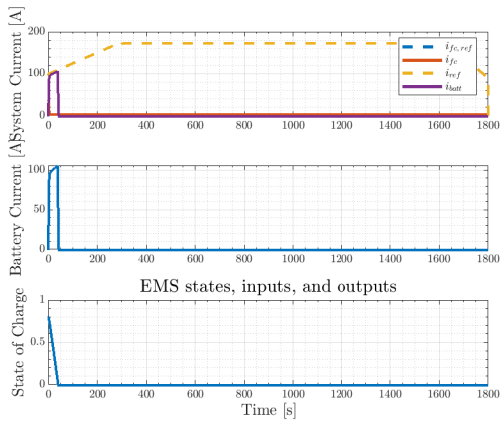

(a) Up: Fuel cell, battery, and load currents during the mission. The battery supplies power during acceleration transients, while the fuel cell dominates during cruise. Middle: Battery current profile. Down: Battery state of charge (SoC) decreasing sharply during initial acceleration.

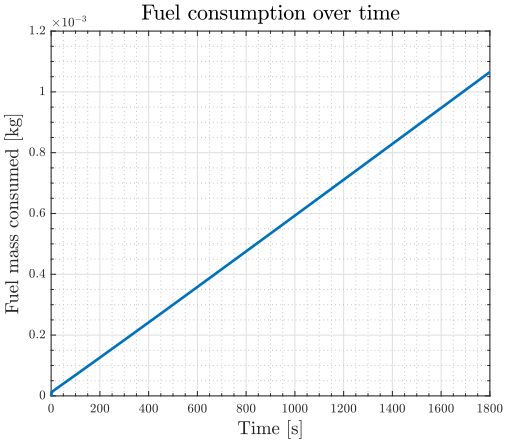

(b) Cumulative hydrogen consumption.

Figure 6.5: Energy Management System Simulation.

The fuel consumption increases linearly with time, which is expected because the fuel cell operates at nearly constant current. The linearity means that the usage of fuel is stable.

The EMS performance shown in Figure 6.5 does not correspond to the goals of this work. The battery is supposed to take on the high current loads, and maintain its state of charge above zero until the airplane reaches the final destination. The simulation is also missing the supercapacitor, which is supposed to also discharge similarly to the battery. Additionally, the linearized model presented in Section 3.3.1 has not been implemented, due to time constraints. This results in the EMS being consisted of very simple models and their relationships with each other, which are not able to properly represent the real system.

Another thing worth mentioning is the fact that the communication between the propulsion system and the EMS is done one way only. This can be noticed by analyzing Figure 6.5a where the battery does not provide any current and the fuel cell provides its optimal current only which is very little compared to the current demand shown in Figure 6.4b. In this case the velocity state should respond to the lack in current provided, and stop following the reference.

7 | Discussion & Conclusion

This chapter is dedicated to discussing the observations made during the simulations, as well as outlining occurring issues, and future developments.

7.1 Discussion

The extent of this work can be split into three main parts: the modeling and control of the aerodynamics, the modeling and control of the energy system components, and the offline optimization used to compute the optimal velocity and fuel cell current references.

The propulsion controller is able to converge with zero steady state error for cruise flight given a certain set of parameters, and the plant is deemed as naturally stable due to the negative A coefficient. However, given different inputs and component minimum and maximum bounds the controller is not always able to follow the reference. There are several contributing factors to why that happens. During the modeling of the aerodynamics, several terms were left constant, such as the propeller efficiency, which is a function of velocity, the thrust and power coefficients, and the parasitic drag coefficient used to compute the constant K_p present in the propulsion power formula, see Equation 4.32. Moreover, due to the lack of a complete physical property overview of the aircraft, low accuracy approximations had to be made to estimate several geometric specifications. Lastly, the collinearity assumption for the acceleration and velocity vectors does not represent the transients, and therefore adds to the increase in error at those time steps.

All of these can be considered as future development steps, as well as using more advanced control techniques such as MPC. Using Model Predictive Control allows the usage of future data, such as future wind predictions, to be able to compute the necessary current demand and adjust the aircraft's velocity given a wind disturbance. The proposed cost function for such a controller is:

$$\begin{aligned} &\arg\min_{i_{ref}, v_{ref}} (\alpha(v - v_{ref})^2 + \beta(i_{ref} - i_{ref_{fc}})^2) \\ &\qquad\qquad\qquad\qquad\qquad\qquad s.t. \\ &\qquad\qquad\qquad\qquad\qquad\qquad v < 0 \\ &\qquad\qquad\qquad\qquad\qquad\qquad 1 \geq SoC \geq 0 \\ &(i_{fc,\,max} + i_{batt,\,max} + i_{sc,\,max}) > i_{ref} \geq 0 \end{aligned} \tag{7.1}$$

where β is a small weight to allow for battery draining, and α should be large to make sure the controller follows the optimal velocity more strictly.

To check for the correctness of the modeling, further tests can be made. One of them is to simulate tail and head wind as a disturbance to the system, and analyze its behavior. This can be done by decreasing or increasing the drag. In case of tail wind, there should be less fuel consumed for the same distance as compared to a total fuel consumption for a flight with no wind. In the case of head wind, the velocity of the aircraft should decrease given the same fuel consumption as with no wind.

The Energy Management System is not able to perform as intended, as the battery gets discharged at the very beginning of the flight. This is believed to happen as a result of an implementation error. As future development the addition of the supercapacitor to the system implementation would be one task. Another improvement would be modeling the fuel cell using a more detailed model [5], as well the modeling of the battery and supercapacitor using the models in [1].

In the context of the offline optimization, the relationship between energy and current at very low currents is not accurate. This is believed to be caused by the same constant approximations in modeling as the ones used for the propulsion system, especially the K_i term and the parasitic drag coefficient C_{D0}. Estimating new values for these terms for each iteration can improve the unstable behavior at low current values. Another thing to consider is the method of finding the optimum values. As described in Section 6.1 the numerical approach does not treat the velocity and current as dependent variables, therefore a method for solving a joint constrained optimization is necessary. The algorithm proposed as a future improvement is called L-BFGS-B, which is known to converge quickly and to handle physics well. Since the objective function given in Equation 5.2 is smooth, i.e. it contains smooth and differentiable terms, L-BFGS-B is a good option, as it is a gradient based method which works best with continuous functions. Moreover, the L-BFGS-B algorithm is capable of handling bounds on the variables [15], and in the case of the EMS, variables such as SoC, V_{sc}, i_{fc} have operational limits. This makes the L-BFGS-B algorithm especially suitable for this kind of problem.

7.2 Conclusion

A hybrid Energy Management System, for an All-Electric Aircraft, is designed in order to distribute a current load between its components: the fuel cell, battery and supercapacitor. The EMS also aims at minimizing the fuel consumption in order to enable the aircraft to fly as long as possible. The EMS system does not work as intended due to the lack of a proper implementation caused on its end by a time constraint. The implemented EMS system does not include a supercapacitor, and neither a proper model for the fuel cell, despite the availability of it's linearized model representation in Section 3.3.1. Furthermore, from the amount of tests that have been done, it is not possible to assess whether the fuel consumption got mini-

mized.

A propulsion controller is designed, implemented and used to follow a desired flight velocity. The output of this controller is a current load that gets input to the EMS controller. Complete physical specifications of the aircraft are necessary for developing an accurate representation of the plant, however such data is scarcely available. The nonlinear model is linearized and the system declared stable.

An offline optimization is also implemented to determine the optimal velocity and fuel cell current references. The relationship between energy loss versus velocity and current, as well as the relationship between velocity and current are modeled. The result of the optimization is acquired numerically, and a gradient based method is suggested as a future development due to its fast convergence and suitability with smooth and differentiable terms.

Bibliography

[1] Souleman Njoya Motapon, Louis-A. Dessaint, and Kamal Al-Haddad. "A Comparative Study of Energy Management Schemes for a Fuel-Cell Hybrid Emergency Power System of More-Electric Aircraft". In: *IEEE Transactions on Industrial Electronics* 61.3 (2014), pp. 1320–1334. DOI: 10.1109/TIE.2013.2257152.

[2] Whitney G. Colella Fritz B. Prinz Ryan O'Hayre Suk-Won Cha. *Fuel Cell Fundamentals*. 3rd. Wiley, 2016.

[3] Or D. Dantsker, Mirco Theile, and Marco Caccamo. "A High-Fidelity, Low-Order Propulsion Power Model for Fixed-Wing Electric Unmanned Aircraft". In: (2018), pp. 1–16.

[4] *TP1350-3SPX25*. URL: https://www.thunderpowerrc.com/products/tp1350-3spx25.

[5] Souleman Njoya M., Olivier Tremblay, and Louis-A. Dessaint. "A generic fuel cell model for the simulation of fuel cell vehicles". In: *2009 IEEE Vehicle Power and Propulsion Conference*. 2009, pp. 1722–1729. DOI: 10.1109/VPPC.2009.5289692.

[6] David A.J. Rand Andrew L. Dicks. *Fuel Cell Systems Explained*. 3rd. Wiley, 2018.

[7] Norman S. Nise. *Control Systems Engineering*. Emea 8th. Wiley, 2019.

[8] *Fuel Cell Efficiency*. https://www.sciencedirect.com/topics/engineering/fuel-cell-efficiency. Accessed: 2025-08-20. ScienceDirect, 2025.

[9] Dr. Alexander Kabza. *Fuel Cell Formulary*. 2019. URL: www.kabza.de.

[10] Barnes W. McCormick. *Aerodynamics, Aeronautics and Flight Mechanics*. Copyright - 1979, by John Wiley Sons, Inc. 1979, p. 652.

[11] Anthony Reinier Hovenburg, Fabio Augusto de Alcantara Andrade, Richard Hann, et al. "Long-Range Path Planning Using an Aircraft Performance Model for Battery-Powered sUAS Equipped With Icing Protection System". In: *IEEE Journal on Miniaturization for Air and Space Systems* 1.2 (2020), pp. 76–89. DOI: 10.1109/JMASS.2020.3003833.

[12] J.B. Brandt, R.W. Deters, G.K. Ananda, et al. *UIUC Propeller Database, Vols 1-4*. https://m-selig.ae.illinois.edu/props/propDB.html. Accessed: 2025-08-20. 2025.

[13] Or Dantsker, Mirco Theile, Marco Caccamo, et al. "Design, Development, and Initial Testing of a Computationally-Intensive, Long-Endurance Solar-Powered Unmanned Aircraft". In: June 2018. DOI: 10.2514/6.2018-4217.

[14] *Model Motors AXi Cyclone 46/760*. URL: https://www.espritmodel.com/axi-cyclone-46-760-inrunner-outrunner-brushless-motor.aspx.

[15] Peihuang Lu Jorge Nocedal Ciyou Zhu Richard H. Byrd. "Algorithm 778: L-BFGS-B: Fortran Subroutines for Large-Scale Bound-Constrained Optimization". In: *ACM Transactions on Mathematical Software* (1997).